iScience

CellPress

Article

A Human Induced Pluripotent Stem Cell-Derived Tissue Model of a Cerebral Tract Connecting Two Cortical Regions

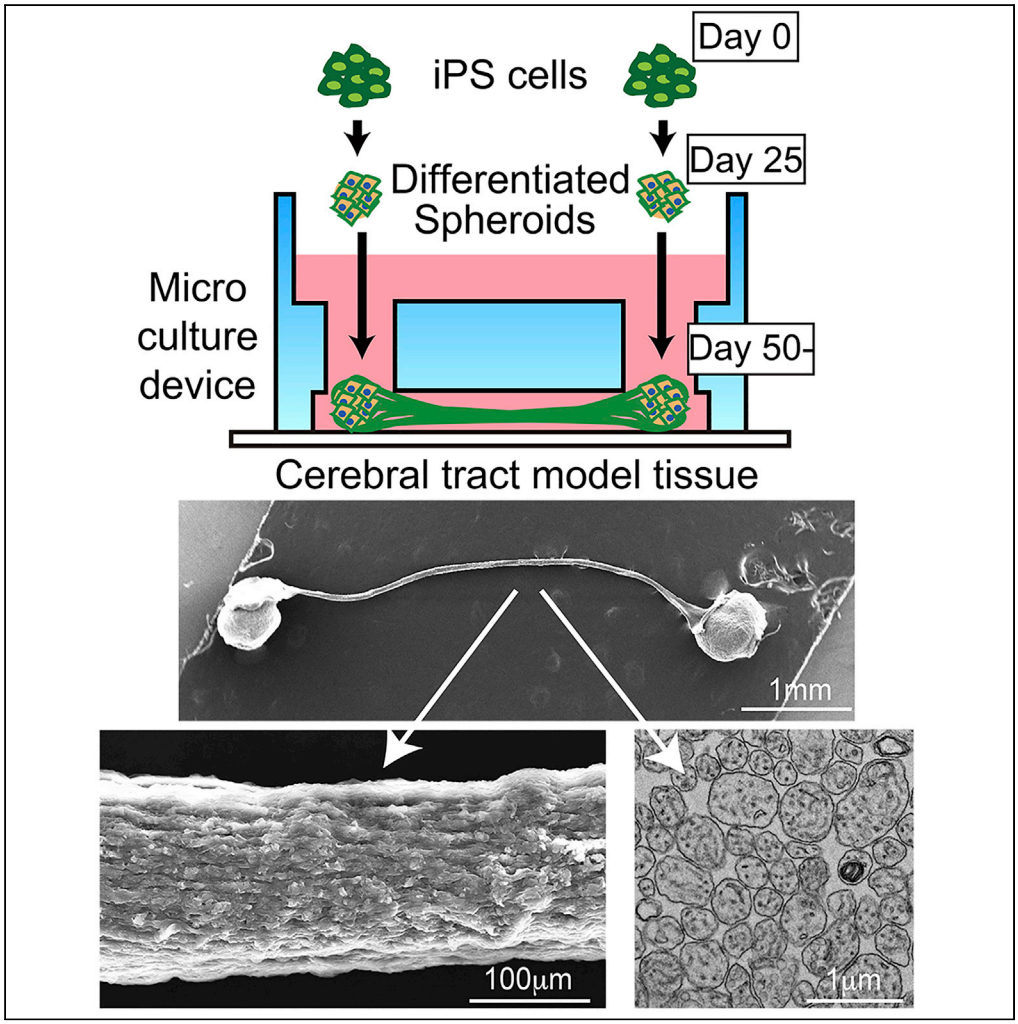

Takaaki Kirihara, Zhongyue Luo, Siu Yu A. Chow, ..., Timothée Levi, Teruo Fujii, Yoshiho Ikeuchi

yikeuchi@iis.u-tokyo.ac.jp

HIGHLIGHTS

A cerebral tract model was generated from iPS cell-derived cortical spheroids

Two spheroids were spontaneously connected with an axon fascicle in a microdevice

An axon fascicle electrically connected two cortical spheroids

Knockdown of L1CAM disrupted axon fascicle formation in the model tissue

Kirihara et al., iScience 14, 301–311
April 26, 2019
https://doi.org/10.1016/j.isci.2019.03.012

iScience

CellPress

Article

A Human Induced Pluripotent Stem Cell-Derived Tissue Model of a Cerebral Tract Connecting Two Cortical Regions

Takaaki Kirihara,[1,2] Zhongyue Luo,[1,2] Siu Yu A. Chow,[1,2] Ryuji Misawa,[1,2] Jiro Kawada,[1] Shinsuke Shibata,[4] Farad Khoyratee,[1,3] Carole Anne Vollette,[1,3] Valentine Volz,[1] Timothée Levi,[1,3] Teruo Fujii,[1] and Yoshiho Ikeuchi[1,2,5,*]

SUMMARY

Cerebral tracts connect separated regions within a brain and serve as fundamental structures that support integrative brain functions. However, understanding the mechanisms of cerebral tract development, macro-circuit formation, and related disorders has been hampered by the lack of an *in vitro* model. Here, we developed a human stem cell-derived model of cerebral tracts, which is composed of two spheroids of cortical neurons and a robust fascicle of axons linking these spheroids reciprocally. In a microdevice, two spheroids of cerebral neurons extended axons into a microchannel between the spheroids and spontaneously formed an axon fascicle, mimicking a cerebral tract. We found that the formation of axon fascicle was significantly promoted when two spheroids extended axons toward each other compared with axons extended from only one spheroid. The two spheroids were able to communicate electrically through the axon fascicle. This model tissue could facilitate studies of cerebral tract development and diseases.

INTRODUCTION

Communication between cortical areas is important for brain functions. Local circuitries in separated regions are interconnected by axons extending from one region to another, which enables the whole brain to function coordinately. Axons connecting distant regions reside in white matter and are structurally organized by bundling into fascicles known as cerebral tracts. Studies of brain anatomy and connectome revealed that a major portion of the axons in cerebral tracts connect two cerebral regions reciprocally (Swanson et al., 2017; Zingg et al., 2014). Cerebral tracts connecting different areas within a hemisphere are called association tracts. Through association tracts, various regions are reciprocally interconnected within a cerebral hemisphere. For example, Wernicke and Broca areas, both of which are associated with language processing, are connected mutually through an association tract called arcuate fasciculus (Bernal and Ardila, 2009; Pujol et al., 2000). Lesion of arcuate fasciculus results in a language disorder known as conduction aphasia. On the other hand, cerebral tracts connecting two cerebral hemispheres are called commissural tracts. Corpus callosum is a commissural tract connecting two hemispheres reciprocally and is the largest axon fascicle in a human brain. Disruption of corpus callosum development causes a disorder known as agenesis of corpus callosum that is associated with diverse symptoms including intellectual disability and cognitive and social deficits (Paul et al., 2007). Despite the anatomical and functional significance of cerebral tracts, still little is known about the mechanisms underlying their formation and organization, largely due to the lack of an *in vitro* model system. Increasing knowledge in brain structures and functions highlights the importance of macro-scale networks and connections between brain regions (Yeh et al., 2018), but few attempts were made to model such large circuitry *in vitro*.

In this article, we report the generation of a model tissue mimicking a cerebral tract. We established a culture of two spheroids with an interconnecting fascicle of axons from human induced pluripotent stem (iPS) cells. We used a tissue culture microdevice equipped with a narrow channel with two chambers at its ends. Two cerebral spheroids were placed into the chambers, and they grew axons reciprocally into the channel. The axons spontaneously formed a robust fascicle, and the two spheroids became connected as one continuous tissue through an axon fascicle. Axons assembled into fascicle significantly faster when two spheroids extended axons reciprocally than when one spheroid extended axons unidirectionally.

[1]Institute of Industrial Science, The University of Tokyo, Tokyo, Japan

[2]Department of Chemistry and Biotechnology, School of Engineering, The University of Tokyo, Tokyo, Japan

[3]Laboratoire de l'Intégration du Matériau au Système (IMS), University Bordeaux, Bordeaux INP, CNRS UMR 5218, Talence, France

[4]Electron Microscope Laboratory, Keio University School of Medicine, Tokyo, Japan

[5]Lead Contact

*Correspondence: yikeuchi@iis.u-tokyo.ac.jp

https://doi.org/10.1016/j.isci.2019.03.012

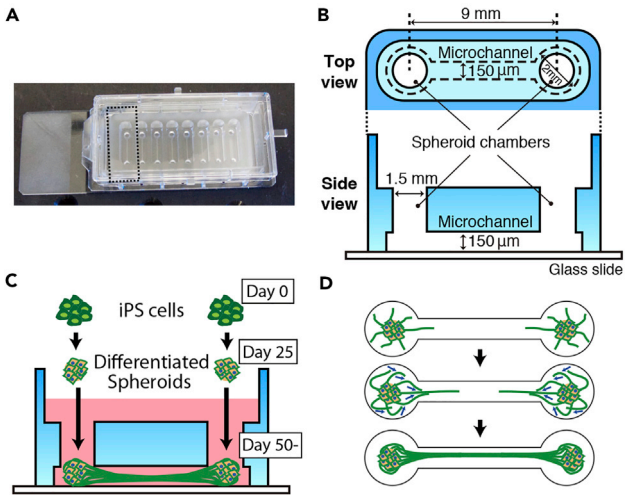

Figure 1. Overview of Cerebral Tract Model Tissue Generated from Human iPS Cells

(A) Photograph showing a microdevice. Dashed region indicates a unit in which one tissue is cultured. Each unit consists of two chambers for spheroids and one narrow channel for axon formation. A maximum of eight tissues can be cultured simultaneously within one microdevice.

(B) Dimensions of the dashed region in (A).

(C) Overview timeline of cerebral tract model tissue generation. Human iPS cells are cultured and differentiated from day 0 (top) until successful differentiation at day 25 (middle). Two differentiated spheroids are then plated into the microdevice and extend axons. The eventual formation of an axon fascicle links the two spheroids, generating the cerebral tract model tissue (bottom).

(D) Schematic illustration of axon fascicle formation process after plating into the microdevice. Initially, single axons extend from both spheroids with a portion growing into the microchannel (top). With time, other axons follow and an increasing number of growing axons enter and reach the middle of the microchannel (middle). From day 50 onward, axons reach the other end of the microdevice and the two spheroids are connected by a robust, straight fascicle (bottom).

Importantly, the two spheroids were electrically connected and coupled through the axon fascicle with distinct response kinetics. The cerebral tract model tissue should provide a promising platform to study the mechanisms underlying cerebral tract development and related diseases.

RESULTS

Generation of a Cerebral Tract Model Tissue

To generate a tissue mimicking a cerebral tract connecting two cortical regions, we provided neurons with a physical environment that facilitates interaction between axons in a narrow channel (Figures 1A and 1B). We differentiated human iPS cells into neurons in three-dimensional spheroids and cultured in the microdevice further to form the tissue (Figure 1C). In the microdevice, the spheroids extend axons into the channel and thereby form a fascicle through interactions between axons (Figure 1D).

We first formed spheroids from human iPS cells with low-adhesive culture vessel and differentiated them into cerebral neurons for 25 days. We confirmed neural differentiation by RT-PCR (Figure 2A). Pluripotent stem cell marker OCT3/4 was decreased, and neural stem cell marker PAX6 and axonal marker L1CAM were increased correspondingly during the differentiation procedure. The expressions of neuronal subtype markers TBR1 and CTIP2 were also increased during the differentiation (Figure 2A). With immunohistochemical analyses, we confirmed that cells in the spheroids were stained with immature neuron marker DCX and neural stem cell marker PAX6 antibodies at day 18 (Figure 2B). We also confirmed that forebrain neural lineage marker FOXG1-positive and Tuj1 (neuron-specific class III beta Tubulin)-positive cells were abundant in the spheroids at day 25 (Figure 2C).

After differentiation, spheroids were transferred into a custom-made culture device. At first, spheroids extended axons within the chambers. After around 10 days of culture in the microdevice (around 35 days total), axons from two spheroids reach the middle of the microchannel (Figure 2D). Around

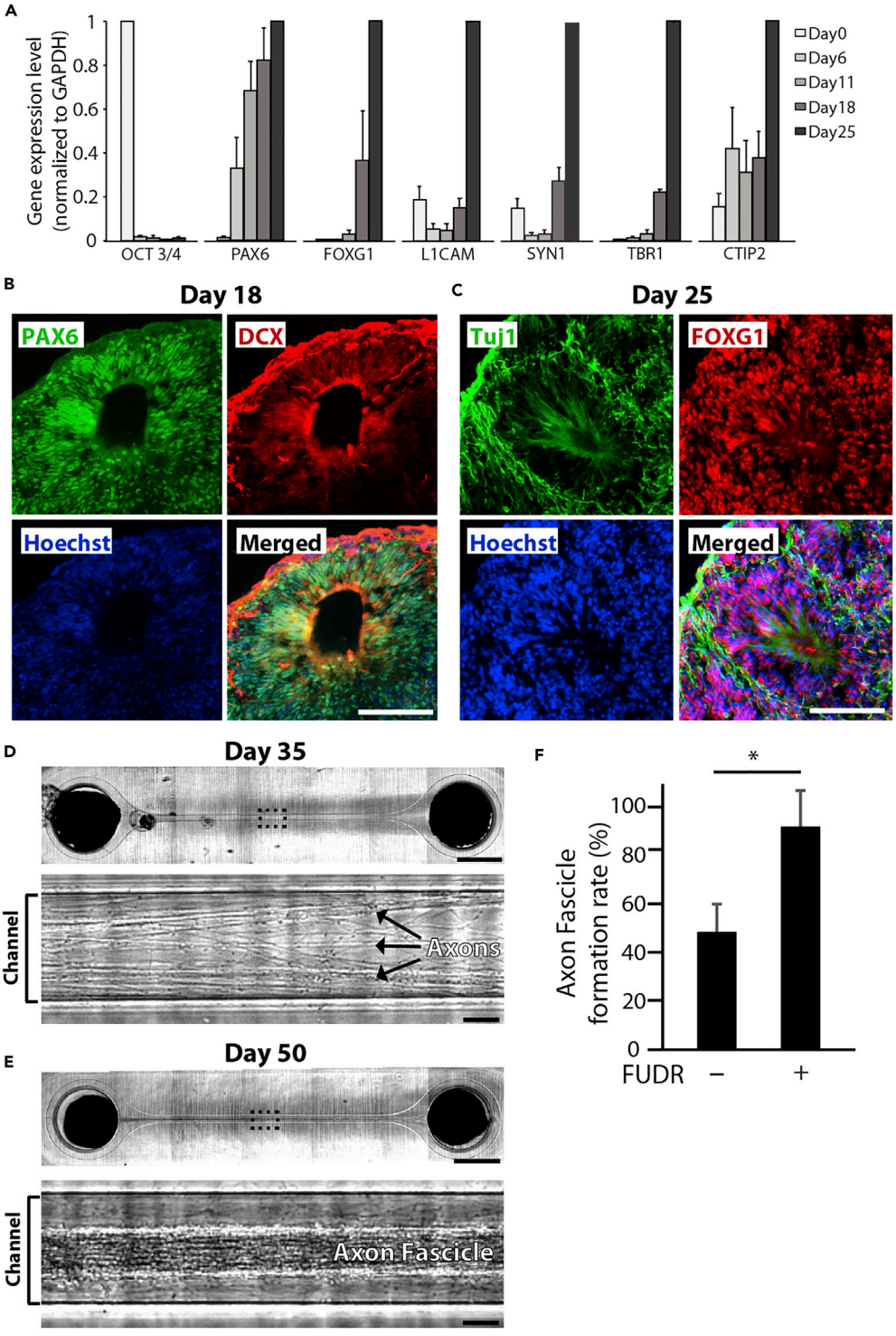

Figure 2. Generation of Spheroids and Cerebral Tract Model Tissue

(A) RT-PCR analyses of spheroid from day 0 to 25.

(B) A representative image of the immunohistochemical analysis of a spheroid with PAX6 antibody (green) and DCX antibody (red) at day 18.

(C) A representative image of the immunohistochemical analysis of a spheroid with Tuj1 antibody (green) and FOXG1 antibody (red) at day 25.

Figure 2. *Continued*

(D and E) Representative bright-field images of spheroids and their axons in a microdevice at days 35 (D) and 50 (E).

(F) Success rate of axon fascicle formation with or without FUDR treatment. The assembled bundle of axons with a diameter of over 25 μm was counted as an axon fascicle. Error bar denotes the standard error of means of values acquired from three independent experiments. In each experiment 8–12 samples were analyzed.

Scale bars: 0.1 mm in (B and C) and 1 mm (top) and 50 μm (bottom) in (D and E). *$p < 0.05$. Error bar denotes SEM.

25 days of culture in a microdevice (around 50 days total), the axons reach the spheroids in opposite side and form a single and straight fascicle within the microchannel (Figure 2E). Sparse labeling of neurons by electroporation with GFP expression plasmid revealed that axons extended from one spheroid reach the spheroid on the other side (Figure S1A). The resultant structure consists of two mutually connected parts: an axon fascicle and spheroids of neurons, which we refer to as the cerebral tract model tissue. When spheroids were placed on a culture surface without our culture device, the spheroids failed to form a single fascicle of axons between them, and instead, extended axons in all directions (Figures S1B and S1C). The efficiency of generating a tissue with a robust axon fascicle was about 50% at day 50 originally (Figure 2F). By treating spheroids with the DNA synthesis inhibitor 5-fluoro-2′-deoxyuridine (FUDR, 40 μM) for 24 h at day 25, the efficiency of axon fascicle formation increased (Figure 2F), suggesting that over-proliferation within spheroids suppresses axon fascicle formation presumably due to congestion at the channel within microdevices. We examined the effect of FUDR treatment by comparing the number of apoptotic cells immunostained with an antibody against cleaved caspase 3 in spheroids with and without FUDR treatment (Figures S1D and S1E). The brief FUDR treatment did not negatively affect the tissue significantly. The success rate was over 80% at day 50 after the optimization, indicating that the formation process of the cerebral tract model tissue is robust and reproducible.

Characterization of a Cerebral Tract Model Tissue

After an axon fascicle was formed, cerebral tract model tissue was retrieved from the culture vessel for various assessments (Figure 3). Whole-mount immunostaining of collected tissues revealed that the axon fascicle was immunoreactive with axonal marker Tau-1 antibody, whereas nuclear staining signals were absent in the axon fascicle (Figure 3A). In contrast, the spheroid was strongly stained with the nuclear dye Hoechst 33342. Further immunohistological analyses of cryosections revealed that the fascicle was stained with Tau-1 antibody and presynaptic protein synapsin I antibody, but not with nuclear dye or dendritic protein MAP2 antibody (Figures 3B and 3C). These data indicate that the fascicle structure formed in the microchannel was made of axons, and not cell bodies or dendrites. The data demonstrated successful organization of the axon fascicle segregated from the spheroids.

To characterize the surface structure of the fascicle, we employed scanning electron microscopic analyses. The surface appeared to be an assembly of axon fibers running in parallel (Figures 3D and 3E). To assess the internal structure, we analyzed the cross-sectional morphology of the fascicle at a higher magnification with transmission electron microscopy (TEM) (Figure 3F). This revealed that axons were packed within the fascicle. Cross sections of well-organized cytoskeletal fibers, including microtubules, were observed within the axons. The average axon diameter measured from TEM images was 338 nm, and its standard deviation was 162 nm (Figure 3G).

Axon Assembly in the Microdevice

We next evaluated axon fascicle assembly in the microdevice. We compared axon fascicles generated from one spheroid with axon fascicles generated between two spheroids (Figure 4). Axon fascicle structure was formed in both cases, suggesting that axons spontaneously extended into the microdevice and formed an axon fascicle without being affected by target cells. Interestingly, we noticed that the axons did not disperse even in the wide neck region in the culture device, when there was a spheroid at both the ends (Figure 4A), whereas axons are dispersed immediately after they exit the microchannel when there was no spheroid at the axon terminus (Figure 4B). We quantitatively analyzed the dispersion of axons at the entry and exit of microchannels (Figure 4C) and verified that axons were dispersed significantly more at the end of fascicle extended from a single spheroid. When a spheroid was placed in a chamber and a glass bead was placed in the other chamber instead of a spheroid, dispersion of axons extended into a chamber with a glass bead was not reduced compared with the axons extended into an empty chamber (Figure S2), suggesting that axons extending in reciprocal directions physically interact

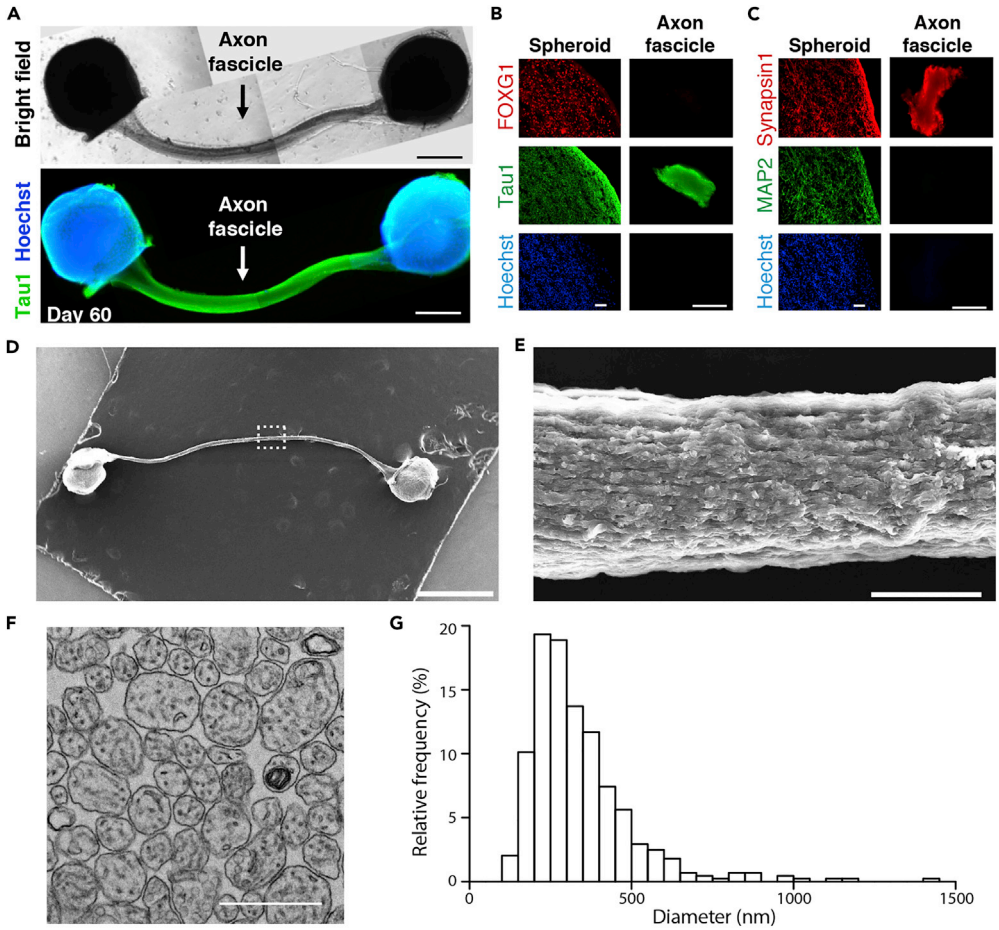

Figure 3. Characterization of the Cerebral Tract Model Tissue

(A) Representative images of a cerebral tract model tissue extracted from the microdevice. Bright-field image (top) and immunostaining with Tau1 antibody (bottom).

(B) Images of cryosections from spheroid (left) and axon fascicle (right) of cerebral tract model tissue stained with Tau1 antibody (top), stained with Hoechst 33342 (middle), and merged (bottom).

(C) Images of cryosections from spheroid (left) and axon fascicle (right) of a cerebral tract model tissue stained with synapsin1 antibody (top), MAP2 antibody (middle), and Hoechst 33342 (bottom).

(D, E) Representative scanning electron microscopic images of axon fascicle. (E) Magnified image of the axon fascicle in the inset in (D).

(F) A representative TEM image of axon fascicle cross section.

(G) Histogram of axon diameters. Measurements were obtained from cross-sectional TEM images of axon fascicles. A total of 445 axons were measured, and the relative frequency was plotted in 50-nm bins.

Scale bars: 0.5 mm in (A), 50 μm in (B and C), 1 mm in (D), 100 μm in (E), and 1 μm in (F).

to facilitate the formation of a bundle. These data suggest that axons can mutually guide opposing axons to reach their target neurons.

Electrical Connections between Two Spheroids by an Axon Bundle

Next, we assessed the electrophysiological functionality of the neurons in the cerebral tract model tissue using calcium indicator dye (Figure 5). When one spheroid was electrically stimulated, the axon fascicle and the connected distal spheroid responded with calcium surge (Figure 5A), indicating that the action potential induced by the stimulation propagated to the axon fascicle and the connected spheroid. When the axon fascicle was cut, calcium surge was detected in the spheroid and connecting axons, but not detected at the distal spheroid and attached axons (Figure S3). Interestingly, we observed delayed response of the distal spheroids compared with the spheroids directly stimulated with electrodes

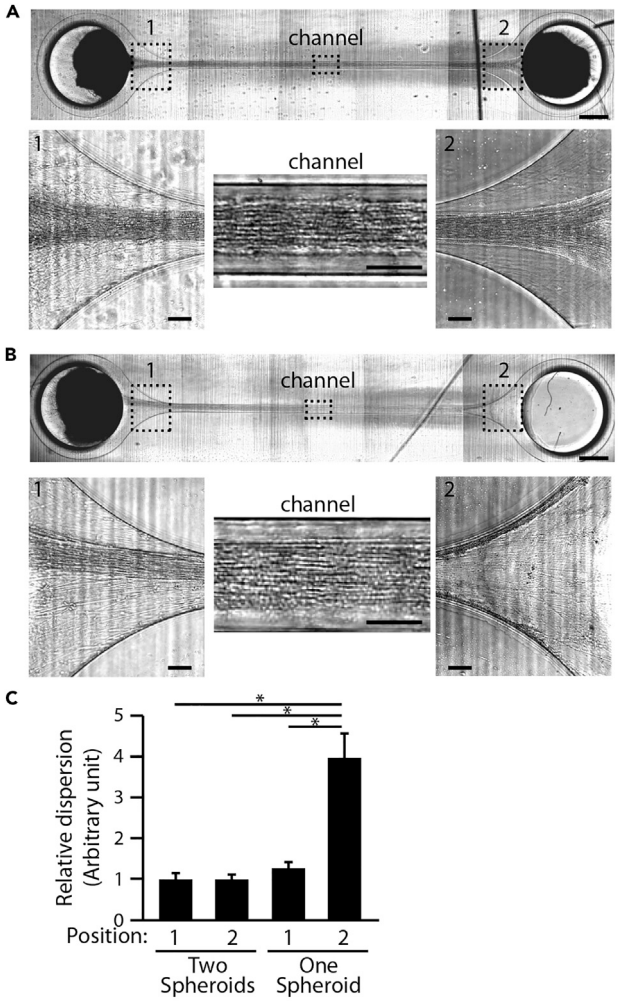

Figure 4. Axon Assembly of Cerebral Tract Model Tissue

(A and B) Representative image of cultured tissue plated with two spheroids (A) and one spheroid (B). Insets are higher-magnification images of entry, center channel, and exit areas within the microdevice.

(C) Relative dispersion of axons in tissues containing one or two spheroids at the entry and exit positions of microdevice. Positions are indicated by 1 and 2, respectively, corresponding to insets in (A) and (B). *$p < 0.001$. A total of 52 images (26 tissues) were analyzed. Error bar denotes SEM.

Scale bars: 0.5 mm (top) and 100 μm (bottom, insets) in (A and B).

(Figure 5B), suggesting that a complex network has been developed within the tissue. These data suggest that axon fascicle conducts electrical activity and macro-scale neural circuits can be formed within cerebral tract model tissues.

Modeling Developmental Cerebral Tract Disorder *In Vitro* by Knockdown of L1CAM

Cerebral tract formation can be disturbed by various factors (Asami et al., 2013; Fortier et al., 2014; Leyva-Díaz and López-Bendito, 2013; McColgan et al., 2018; Rose et al., 2000). L1CAM gene produces L1 cell adhesion molecule that facilitates axons to interact with each other (Siegenthaler et al., 2015; Wiencken-Barger et al., 2004). Mutations in L1CAM cause agenesis of corpus callosum (ACC) (Demyanenko et al., 1999; Edwards et al., 2014; Fransen et al., 1995). To model the developmental defect of cerebral tract formation including ACC, we knocked down L1CAM gene in cells in our model tissue (Figure 6) using a validated RNAi construct (Figure S4). Axons from the L1CAM knockdown cells exhibited significantly lower ratio of axons assembled into a bundle than the control cells (Figure 6C). These data suggest that the axon fascicle formation process in our tissue is relevant to cerebral tract formation *in vivo* and that the tissue can be used to model developmental disease related to cerebral tract.

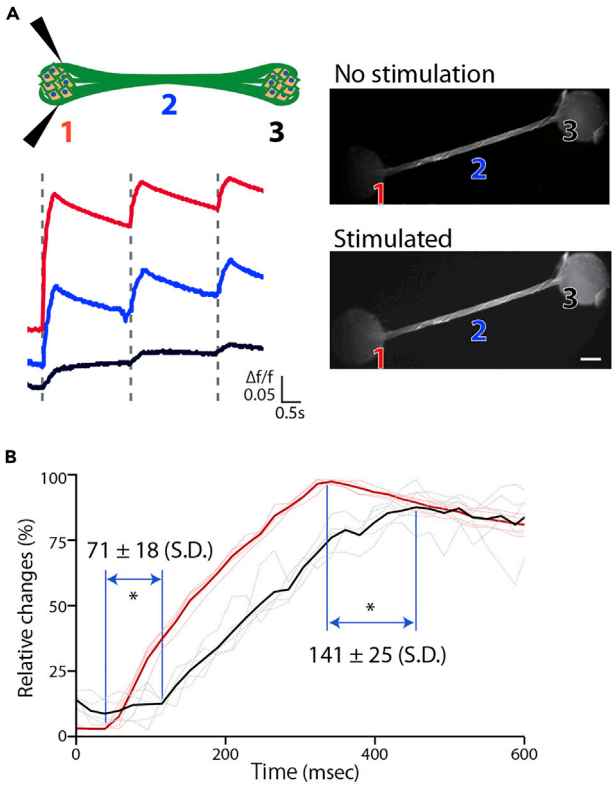

Figure 5. Calcium Response of Cerebral Tract Model Tissue to Electrical Stimulations

(A) Schematics and representative images of calcium imaging with electrical stimulation. Dashed lines indicate stimulations.

(B) Enlarged plots of calcium imaging peaks. The red and black curves indicate relative calcium imaging intensity changes on the stimulated spheroids, and the connected distal spheroids, respectively. Solid lines are average of five independent curves indicated by dotted lines.

Error bar denotes SEM. *$p < 0.001$. Scale bar, 0.5 mm in (A).

DISCUSSION

In this study, we established a method to generate a stem cell-derived tissue that mimics the structure of reciprocally connected cortical regions. We differentiated human iPS into cerebral spheroids and transferred them into our microdevice. The spheroids extended axons into a microchannel where the axons formed a bundle structure. The axon bundle connects the two spheroids, and the resultant tissue contains two spheroids interconnected with an axon fascicle. The axon fascicle can transmit electrical activity from one spheroid to another within the tissue. We observed that axon fascicle formation was significantly promoted when a target spheroid is present.

We provided neurons with spatial instructions using a microdevice to form the tissue modeling cortical connections. Based on our previous study demonstrating that axons of human iPS cell-derived motor neurons can form a robust fascicle when they grow in a narrow and long channel without molecular guidance (Kawada et al., 2017), we employed the strategy of providing only spatial instructions to generate the cerebral tract model tissue. In the case with motor neurons, axons extended unidirectionally in a microchannel from cells in one chamber and spontaneously formed a nerve-mimicking tissue (also referred as a nerve organoid) without molecular instructions. In this study, we demonstrated that axons of cerebral neurons assemble into a fascicle in a narrow channel, suggesting that the spontaneous assembly of axons is not a neuronal-subtype-specific event, and that multiple cell types share common mechanisms to form the bundle structure.

Two spheroids are connected by an axon fascicle in the generated tissues. We did not observe cell bodies or dendrites in the fascicle, suggesting that the two spheroids are purely connected by axons

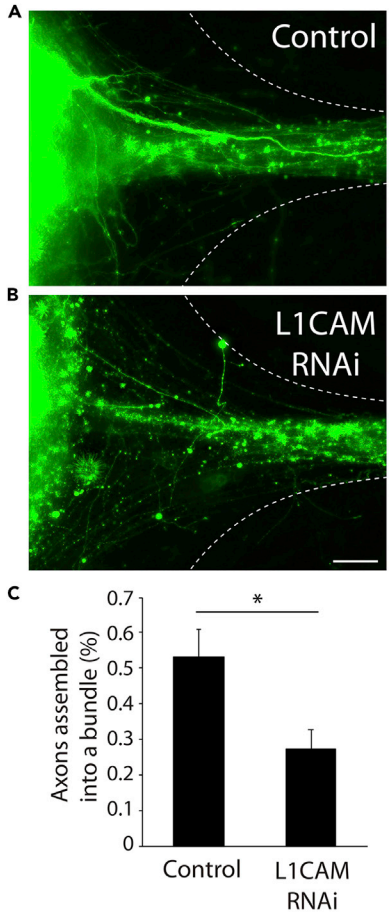

Figure 6. Knockdown of L1CAM in the Generated Tissue

(A) Neurons in a tissue were electroporated with control scrambled plasmid together with GFP expression plasmid. Broken lines indicate the edges of culture chamber.

(B) Neurons were electroporated with L1CAM RNAi plasmid together with GFP expression plasmid.

(C) The percentage of axons assembled into a bundle was analyzed in tissues electroporated with the control scrambled plasmid or L1CAM RNAi plasmid.

Scale bars, 0.1 mm in (A and B). Error bar denotes SEM. *$p < 0.05$. Independently prepared five control samples and four knockdown samples were analyzed.

extended toward each other. The surface and cross section observation of the fascicles revealed that axons were tightly packaged and organized in parallel. The axon diameter histogram displayed a single peak distribution, and the mean diameter was 338 $\pm$ 162 nm (standard deviation). Within the human brain, cerebral tracts *in vivo* displayed a similar axonal diameter distribution pattern to our *in vitro* model tissue, with a larger mean value of 450–820 nm (Liewald et al., 2014). The difference might be due to the immature state of human iPS cell-induced neurons in the tissue. The cross-sectional image (Figure 3F) anatomically resembles unmyelinated immature cerebral tract in a guinea pig (Perge et al., 2012), a rhesus monkey (LaMantia and Rakic, 1990), and a mouse (Miyazaki et al., 2014). Although it is immature and lacks various key steps in cerebral tract development (e.g., myelination, pruning, and midline crossing), our tissue recapitulates axon fasciculation, which is the most fundamental process. The tissue presented in this work can provide a platform to assess the further developmental processes in the future.

Numerous regions are connected with each other through extended axons in a cerebral cortex (Swanson et al., 2017; Zingg et al., 2014). Reciprocal connections between two regions are frequently observed in the cerebral cortex, but it is unclear how these mutual connections are formed between two appropriate

regions within a hemisphere or between hemispheres. In our microdevice, two spheroids of neurons extended axons toward each other and assembled into a fascicle. Notably, the reciprocally extended axons assembled tighter fascicle throughout the span, whereas single spheroid formed an axon fascicle with a dispersed ending. We did not see similar effect by a glass bead, suggesting that interaxonal interaction is required for efficient axon fascicle formation. These observations imply that axons could guide opposing axons to their cell body region, thus naturally facilitating reciprocal connections between two regions. The model tissue can be used to study cerebral tract formation mechanisms by numerous tools, including genetic manipulations and live imaging.

We stimulated one spheroid and observed that the axon fascicle and connected distal spheroid responded with a calcium surge. The distal spheroid did not respond to stimulations when the axon fascicle was cut, indicating that the axon fascicle transduces action potential to the connected spheroid (Figure S3B). Strikingly, the calcium signal of the distal spheroid responded slightly slower than the spheroid directly stimulated (Figure 5B). This implies that the distal spheroid took extra time to fire action potentials owing to delay of axonal transmissions, or synaptic transmissions. Unmyelinated axons with a small diameter (<1 μm) conduct action potential at 0.3–2 m/s (Waxman and Bennett, 1972). Given that the axon bundles in our tissue are about 7 mm, they could produce 3.5- to 23-ms axonal delay. In addition, a single synaptic transmission causes a 0.4- to 4-ms delay (Katz and Miledi, 1965). As the observed delay was larger than those combined, it suggests that slower calcium kinetics or multi-cellular circuit activation in the tissue contributed to the observed delay. *In vivo* experiments reported that direct response to electrical stimulation displays 10- to 50-ms delay, and secondary response follows with 50- to 500-ms delay at a distal site within the brain (Entz et al., 2014). As the secondary response is considered to be triggered through complex circuit activation, the *in vivo* observation supports the idea of complex network activity in our model tissue.

By knocking down the L1CAM gene known to be associated with cerebral tract malformation disease, the tissue was used to model developmental disorders. Consistent with the molecular function of L1CAM protein in axo-axonal interaction, we observed less efficient assembly of axons extended from a spheroid electroporated with L1CAM RNAi construct than control. This demonstrates that our tissue can be used to model developmental disorders and further implies that the axon assembly process is relevant for cerebral tract development *in vivo*.

The model tissue of cerebral tract connecting two cerebral regions was established in this study, which provided a method to create and evaluate macro-scale neural network between cerebral cortex regions. The model can provide a platform to investigate cerebral tract development, circuit formation, and related diseases. To build a better model that recapitulates brain circuitry, it would be necessary to further develop the model, e.g., by myelination and formation of a complex neural circuit in the future.

Limitations of the Study

We utilized a culture device made with polydimethylsiloxane (PDMS) to provide physical instructions to the cells in our study. PDMS has been widely used for biological studies, because it is biocompatible, inert, and easy to shape by photolithography techniques. Because of the flexibility of design, our model tissue can be modified by changing the dimensions of the culture device to alter the length of axon bundles, and the number of spheroids, which can allow further studies on network properties of the neuronal tissue. A negative side of the PDMS device is that it does not physically expand along with the expansion of the spheroids. Owing to this limitation, we employed brief treatment with FUDR to limit the proliferation of cells in our model tissue, so that the spheroids do not overgrow and fill out the culture device. Usage of FUDR in turn limits the size of the spheroid in our system, and could affect the development of the spheroids in long term. To overcome the limitation of the current method, it will be interesting to make a culture device with materials that can expand as the spheroids grow within the device, ultimately mimicking the development of a skull that expands as a brain grows inside.

METHODS

All methods can be found in the accompanying Transparent Methods supplemental file.

SUPPLEMENTAL INFORMATION

Supplemental Information can be found online at https://doi.org/10.1016/j.isci.2019.03.012.

ACKNOWLEDGMENTS

We thank Dr. Naoko Yoshie, Dr. Shintaro Nakagawa, and Mr. Kyungmo Sung for providing equipment and assistance for SEM analyses. We also thank Mr. Christian Felsner, Dr. Miles Pennington, and members of RCA-IIS design lab for discussion. This work was supported by Japan Society for the Promotion of Science (JSPS) Grants-in-Aid for Scientific Research 17H05661 and 18K19903 (Y.I.), by CASIO Science Promotion Foundation (Y.I.), by Tanaka Memorial Foundation (Y.I.), and by a Grant for Brain Mapping by Integrated Neurotechnologies for Disease Studies (Brain/MINDS) by AMED under the Grant Number JP18dm0207002 (S.S.).

AUTHOR CONTRIBUTIONS

T.K. established the culture protocol. Y.I., J.K., and T.F. designed the microdevice. T.K., Z.L., S.Y.A.C., and R.M. characterized the cells and the cultured tissues. S.S. and A.C. performed the electron microscopy analyses. Z.L., F.K., C.A.V., V.V., and T.L. performed calcium imaging. T.K. and Y.I. wrote the manuscript. Y.I. designed the study.

DECLARATION OF INTERESTS

The authors declare no competing financial interest in this work.

Received: June 29, 2018
Revised: December 13, 2018
Accepted: March 11, 2019
Published: April 18, 2019

REFERENCES

Katz, B., and Miledi, R. (1965). The measurement of synaptic delay, and the time course of acetylcholine release at the neuromuscular junction. Proc. R. Soc. Lond. B Biol. Sci. *161*, 483–495.

Asami, T., Saito, Y., Whitford, T.J., Makris, N., Niznikiewicz, M., McCarley, R.W., Shenton, M.E., and Kubicki, M. (2013). Abnormalities of middle longitudinal fascicle and disorganization in patients with schizophrenia. Schizophr. Res. *143*, 253–259.

Bernal, B., and Ardila, A. (2009). The role of the arcuate fasciculus in conduction aphasia. Brain *132*, 2309–2316.

Demyanenko, G.P., Tsai, A.Y., and Maness, P.F. (1999). Abnormalities in neuronal process extension, hippocampal development, and the ventricular system of L1 knockout mice. J. Neurosci. *19*, 4907–4920.

Edwards, T.J., Sherr, E.H., Barkovich, A.J., and Richards, L.J. (2014). Clinical, genetic and imaging findings identify new causes for corpus callosum development syndromes. Brain *137*, 1579–1613.

Entz, L., Tóth, E., Keller, C.J., Bickel, S., Groppe, D.M., Fabó, D., Kozák, L.R., Erőss, L., Ulbert, I., and Mehta, A.D. (2014). Evoked effective connectivity of the human neocortex. Hum. Brain Mapp. *35*, 5736–5753.

Fortier, C.B., Leritz, E.C., Salat, D.H., Lindemer, E., Maksimovskiy, A.L., Shepel, J., Williams, V., Venne, J.R., Milberg, W.P., and McGlinchey, R.E. (2014). Widespread effects of alcohol on white matter microstructure. Alcohol Clin. Exp. Res. *38*, 2925–2933.

Fransen, E., Lemmon, V., Van Camp, G., Vits, L., Coucke, P., and Willems, P.J. (1995). CRASH syndrome: clinical spectrum of corpus callosum hypoplasia, retardation, adducted thumbs, spastic paraparesis and hydrocephalus due to mutations in one single gene, L1. Eur. J. Hum. Genet. *3*, 273–284.

Kawada, J., Kaneda, S., Kirihara, T., Maroof, A., Levi, T., Eggan, K., Fujii, T., and Ikeuchi, Y. (2017). Generation of a motor nerve organoid with human stem cell-derived neurons. Stem Cell Reports *9*, 1441–1449.

LaMantia, A., and Rakic, P. (1990). Axon overproduction and elimination in the corpus callosum of the developing rhesus monkey. J. Neurosci. *10*, 2156–2175.

Leyva-Díaz, E., and López-Bendito, G. (2013). In and out from the cortex: development of major forebrain connections. Neuroscience *254*, 26–44.

Liewald, D., Miller, R., Logothetis, N., Wagner, H.J., and Schüz, A. (2014). Distribution of axon diameters in cortical white matter: an electron-microscopic study on three human brains and a macaque. Biol. Cybern. *108*, 541–557.

Miyazaki, H., Oyama, F., Inoue, R., Aosaki, T., Abe, T., Kiyonari, H., Kino, Y., Kurosawa, M., Shimizu, J., Ogiwara, I., et al. (2014). Singular localization of sodium channel β4 subunit in unmyelinated fibres and its role in the striatum. Nat. Commun. *5*, 5525.

McColgan, P., Gregory, S., Seunarine, K.K., Razi, A., Papoutsi, M., Johnson, E., Durr, A., Roos, R.A.C., Leavitt, B.R., Holmans, P., et al. (2018). Brain regions showing white matter loss in huntington's disease are enriched for synaptic and metabolic genes. Biol. Psychiatry *83*, 456–465.

Perge, J.A., Niven, J.E., Sterling, P., Mugnaini, E., and Balasubramanian, V. (2012). Why Do Axons Differ in Caliber? J. Neurosci. *32*, 626–638.

Paul, L.K., Brown, W.S., Adolphs, R., Tyszka, J.M., Richards, L.J., Mukherjee, P., and Sherr, E.H. (2007). Agenesis of the corpus callosum: genetic, developmental and functional aspects of connectivity. Nat. Rev. Neurosci. *8*, 287–299.

Pujol, J., Bello, J., Deus, J., Cardoner, N., Martí-Vilalta, J.L., and Capdevila, A. (2000). Beck Depression Inventory factors related to demyelinating lesions of the left arcuate fasciculus region. Psychiatry Res. *99*, 151–159.

Rose, S.E., Chen, F., Chalk, J.B., Zelaya, F.O., Strugnell, W.E., Benson, M., Semple, J., and Doddrell, D.M. (2000). Loss of connectivity in Alzheimer's disease: an evaluation of white matter tract integrity with colour coded MR diffusion tensor imaging. J. Neurol. Neurosurg. Psychiatry *69*, 528–530.

Siegenthaler, D., Enneking, E.M., Moreno, E., and Pielage, J. (2015). L1CAM/Neuroglian controls the axon-axon interactions establishing layered and lobular mushroom body architecture. J. Cell Biol. *208*, 1003–1018.

Swanson, L.W., Hahn, J.D., and Sporns, O. (2017). Organizing principles for the cerebral cortex network of commissural and association connections. Proc. Natl. Acad. Sci. U S A *114*, E9692–E9701.

Waxman, S.G., and Bennett, M.V. (1972). Relative conduction velocities of small myelinated and non-myelinated fibres in the central nervous system. Nat. New Biol. *238*, 217–219.

Wiencken-Barger, A.E., Mavity-Hudson, J., Bartsch, U., Schachner, M., and Casagrande, V.A. (2004). The role of L1 in axon pathfinding and fasciculation. Cereb. Cortex *14*, 121–131.

Yeh, F.C., Panesar, S., Fernandes, D., Meola, A., Yoshino, M., Fernandez-Miranda, J.C., Vettel, J.M., and Verstynen, T. (2018). Population-averaged atlas of the macroscale human structural connectome and its network topology. Neuroimage *178*, 57–68.

Zingg, B., Hintiryan, H., Gou, L., Song, M.Y., Bay, M., Bienkowski, M.S., Foster, N.N., Yamashita, S., Bowman, I., Toga, A.W., et al. (2014). Neural networks of the mouse neocortex. Cell *156*, 1096–1111.

ISCI, Volume *14*

Supplemental Information

A Human Induced Pluripotent Stem Cell-Derived Tissue Model of a Cerebral Tract Connecting Two Cortical Regions

Takaaki Kirihara, Zhongyue Luo, Siu Yu A. Chow, Ryuji Misawa, Jiro Kawada, Shinsuke Shibata, Farad Khoyratee, Carole Anne Vollette, Valentine Volz, Timothée Levi, Teruo Fujii, and Yoshiho Ikeuchi

Supplemental Information

A human iPS cell-derived tissue model of a cerebral tract connecting two cortical regions

Takaaki Kirihara, Zhongyue Luo, Siu Yu A. Chow, Ryuji Misawa, Jiro Kawada, Shinsuke Shibata, Farad Khoyratee, Carole Anne Vollette, Valentine Volz, Timothée Levi, Teruo Fujii, Yoshiho Ikeuchi

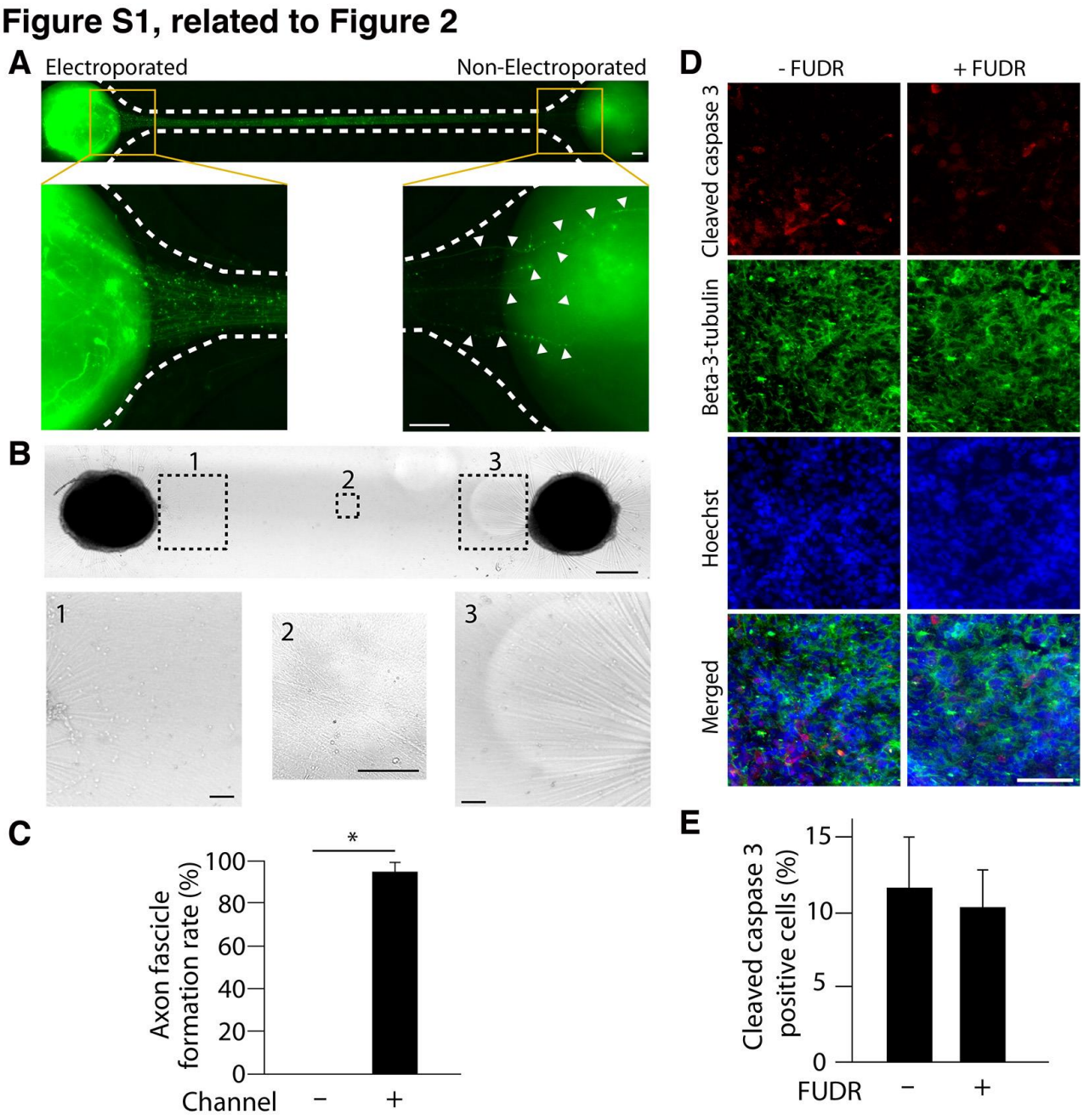

Figure S1, related to Figure 2

(A) Neurons in a spheroid on one side of a tissue in a microdevice were electroporated with GFP expression plasmid and extended axons toward a non-electroporated spheroid on the other end. Dashed lines indicate the edges of culture chamber. Arrowheads indicate distal axon terminals reached to the target spheroid. (B) Two spheroids placed on a flat surface coated with Matrigel did not form axon fascicle between them. (C) The percentage of attempts that formed axon fascicle between two spheroids placed in our microdevice or on a flat surface. Three independent experiments were analyzed. (D) Sections of spheroids treated with or without FUDR were stained with antibodies against cleaved caspase 3 and beta-3-tubulin, and Hoechst. (E) The percentage cleaved caspase 3-positive cells in spheroids treated with or without FUDR. Four control and four FUDR-treated spheroids were analyzed. Scale bar: (A, B, D) 0.1 mm. Error bar denotes standard error of means (SEM).

Figure S2, related to Figure 4

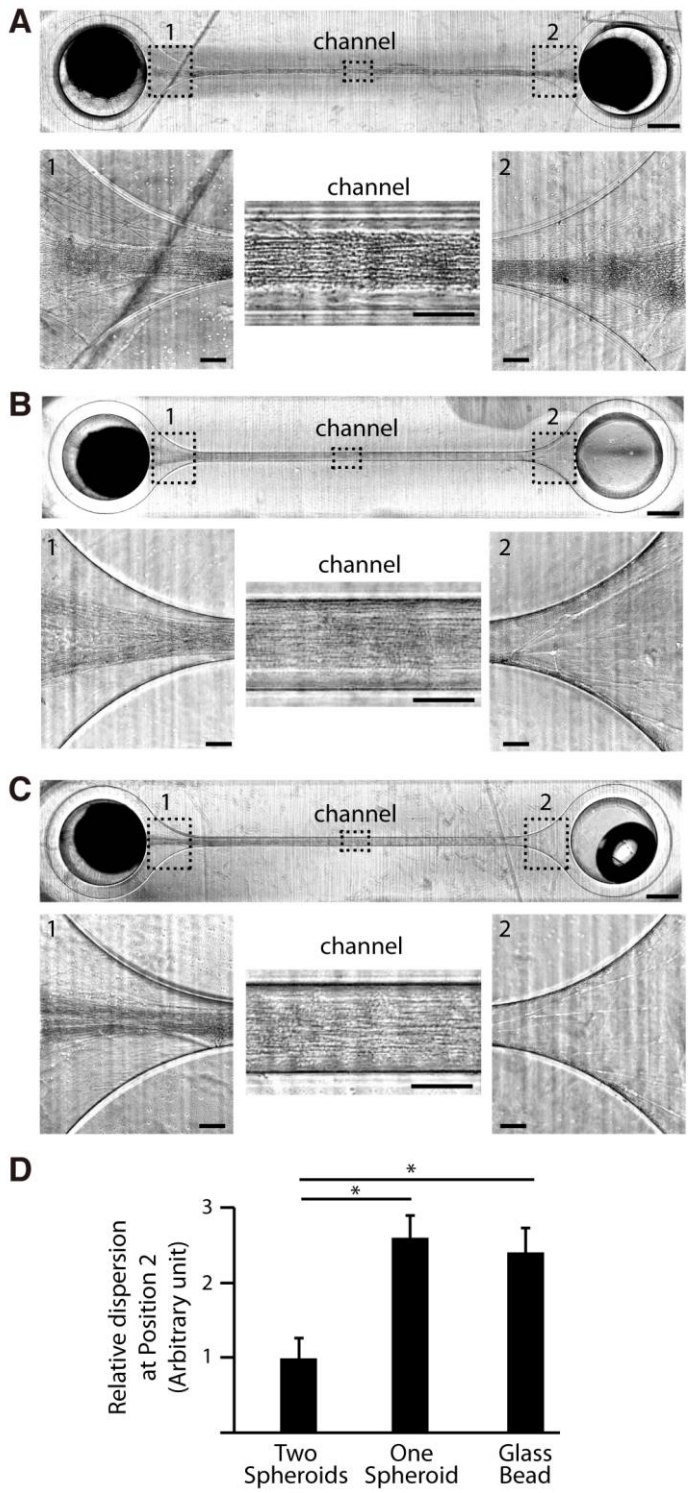

Figure S2, related to Figure 4

(A, B, C) Representative image of cultured tissue plated with two spheroids (A), one spheroid (B), and one spheroid with one glass bead (C). Insets are higher magnification images of entry, center channel, and exit areas within the microdevice. (D) Relative dispersion of axons in tissues containing one or two spheroids at the exit position of microdevice (position 2). Asterisk denotes $p < 0.05$. A total of 18 samples were analyzed. Error bar denotes standard error of means (SEM). Scale bars: (A, B) Top: 0.5 mm, Bottom (Insets): 100 µm.

Figure S3, related to Figure 5

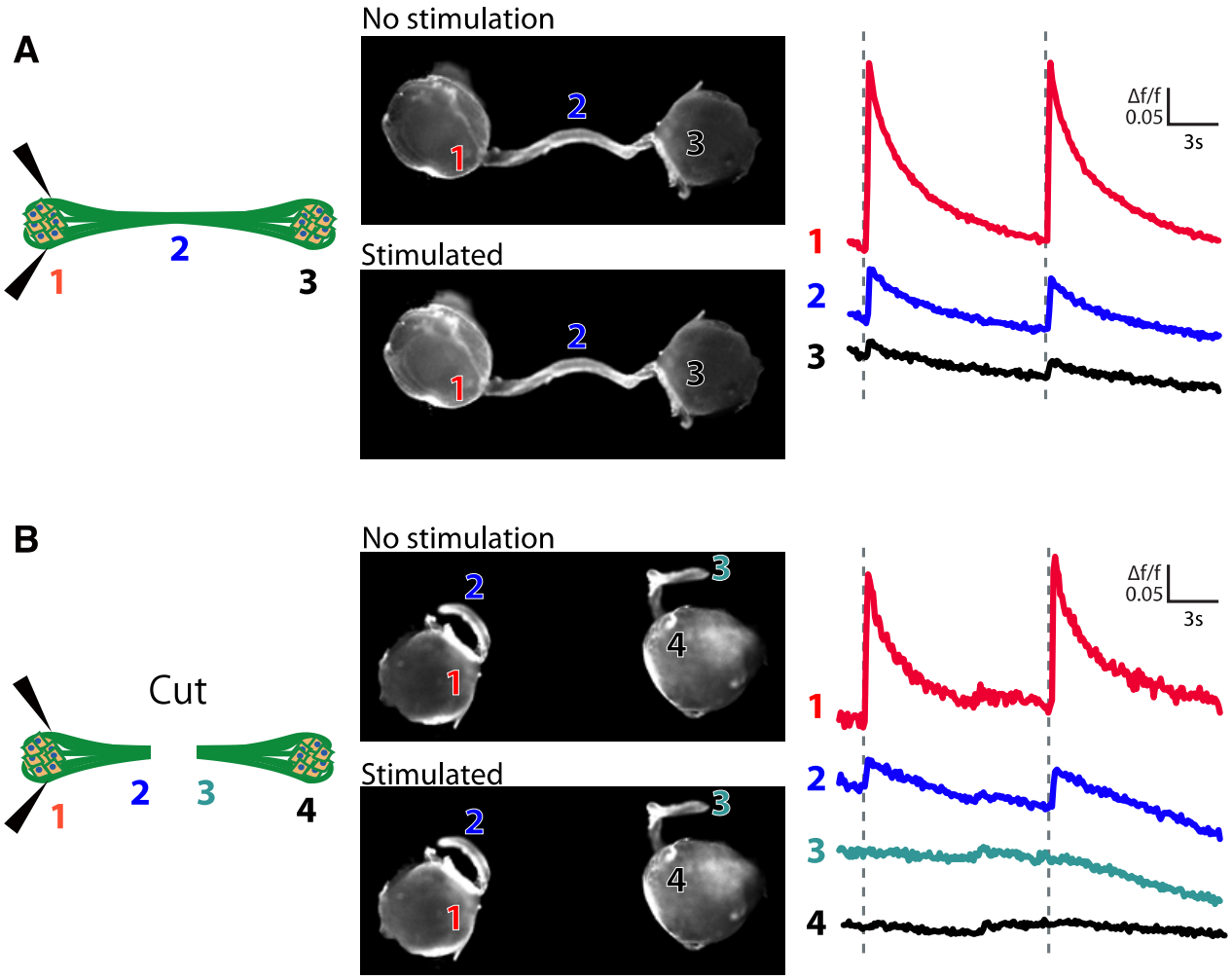

Figure S3, related to Figure 5

(A, B) Schematics and representative images of calcium imaging with electrical stimulation of intact (A) and cut (B) tissue. Dashed lines indicate stimulations.

Figure S4, related to Figure 6

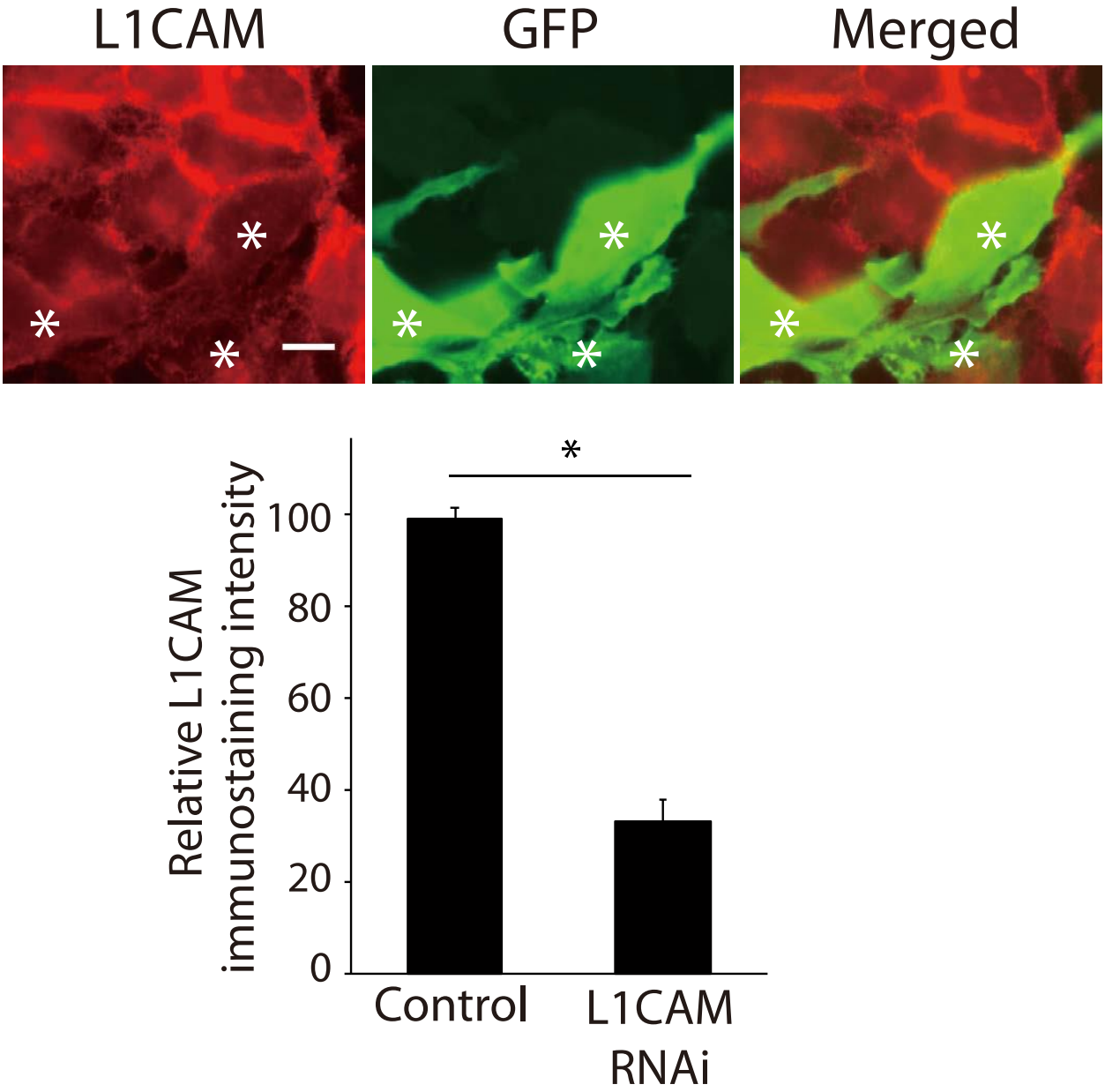

Figure S4, related to Figure 6

(A) Representative images of HEK293T cells transfected with L1CAM RNAi plasmid together with GFP expression plasmid. The GFP-positive transfected cells exhibited weaker staining of L1CAM. (B) Relative L1CAM immunostaining intensity was quantified. L1CAM staining intensity was significantly lower in the GFP-positive transfected cells than the GFP-negative non-transfected cells. Asterisks denote $p < 0.001$. Error bar denotes standard error of means (SEM). Scale bar: (A) 10 µm.

Transparent Methods

Human iPS cells

409B2 human iPS cell line was provided by Kyoto University through RIKEN Bioresource center cell bank (HPS0076) (Okita et al., 2011). The iPS cells were cultured in Essential 8 medium (Thermo Fisher Scientific) on a dish coated with vitronectin (VTN-N, Thermo Fisher Scientific) to maintain the undifferentiated state.

Cerebral spheroid generation

Three dimensional spheroids of cerebral neurons were generated according to previously published methods with modifications (Lancaster et al., 2013). We adapted the protocol of making cerebral organoid to generate neural spheroids accordingly. Human iPS cells were dissociated with TrypLE (Thermo Fisher Scientific), and transferred into low-adhesion U bottom 96-well plate (Sumitomo Bakelite) with Essential 6 medium with ROCK inhibitor Thiazovivin (1 μM, Tocris) and basic fibroblast growth factor (FGF2, 4 ng/mL, Pepro Tech) at a density of 10,000 cells per well. The medium was partially replaced every other day. FGF2 and thiazovivin was added only for first 4 days. Inhibitor of BMP (Dorsomorphin: 5 uM) and TGFb signaling pathway (SB421542: 10 uM) were added from day 2 to day 6 to enhance neural differentiation of iPS cells. On day 6, spheroids were transferred to non-treated dish (Iwaki) in N2 medium [DMEM/F12 medium supplemented with 1% N2 supplement, Glutamax, nonessential amino acids (NEAA) and penicillin-streptomycin (PS) (Thermo Fisher Scientific) insulin (2.5 mg/L), Mercaptoethanol (3.5 uL/L)] for 5 days. On day 11, the spheroids were transferred to differentiation medium [DMEM/F12 and Neurobasal medium (1:1 mix) supplemented with 1% B27 supplement without Vitamin A, 0.5% N2 supplement, Glutamax, NEAA and PS] and cultured further for 14 days. A spheroid was placed in a well to prevent spheroid from fusing physically. On day 15. culture medium was changed to differentiation medium with vitamin A and cultured further for 10 days before transferring into device.

Microdevice for tissue culture

The culture device was fabricated at Fukoku Bussan, Japan by a standard transfer molding process. Polydimethylsiloxane (PDMS) transferred to a metal mold was heated, and the device was taken out of the mold. Prior to tissue culture, devices were placed on glass slides, disinfected with 70% ethanol and dried for usage.

Inside of culture devices was coated with Matrigel (growth factor reduced, Corning) diluted at 1:50 with DMEM (Sigma Aldrich). The coating solution was replaced by differentiation medium supplemented with 20 ng/mL brain-derived neurotrophic factor (BDNF), and then the spheroids were transferred into the culture device. The day before the transfer, we treated the spheroids with 40μM FUDR for 24 hours unless otherwise stated. A half of the culture medium was replaced with fresh medium every 3 days during the culture in the microdevices. Typically, 20-30 days after

spheroids were transferred into the device, an axon fascicle connected two spheroids within the microdevice.

RT-PCR

RNA was isolated with TriPure isolation reagent (Roche), and cDNA was prepared by reverse transcription using SuperScript Ⅳ (Life Technologies). Quantitative PCR was performed with KAPA SYBR Fast (Kapa Biosystems) on CFX connect (Bio-Rad). The following primer pairs were used: GAPDH-F: 5'-ACCACAGTCCATGCCATCAC-3' and GAPDH-R: 5'-TCCACCACCCTGTTGCTGTA-3'; OCT3/4-F: 5'-GAGCAAAACCCGGAGGAGT-3' and OCT3/4-R: 5'-TTCTCTTTCGGGCCTGCAC-3'; PAX6-F: 5'-ATCGAAGGGCCAAATGGAGA-3' and PAX6-R: 5'-GGAGTATGAGGAGGTCTGGC-3'; FOXG1-F: 5'-TGGCCCATGTCGCCCTTCCT-3' and FOXG1-R: 5'-GCCGACGTGGTGCCGTTGTA-3'; L1CAM-F: 5'-ACACACAACCTGACCGATCT-3' and L1CAM-R: 5'-ACATACTGTGGCGAAAGGGA-3'; SYN1-F: 5'-GGTCATTGGGCTGCAGTATG-3' and SYN1-R: 5'-TGGCATACGTCTTGGTCAGT-3'; TBR1-F: 5'-CTCAGTTCATCGCCGTCACC-3' and TBR1-R: 5'-AGCCGGTGTAGATCGTGTCATA-3'; CTIP2-F: 5'-GAGTACTGCGGCAAGGTGTT-3' and CTIP2-R: 5'- TAGTTGCACAGCTCGCACTT-3'.

Immunostaining and image analyses

Tissues were pre-fixed with 4% paraformaldehyde/PBS and 4% sucrose solution for 15 min. Tissues extracted from the device were fixed with the same solution for 30 min at room temperature, and subsequently subjected to immunostaining directly or cryosectioning followed by immunostaining. After three washes with PBS, the tissue or cryosections were incubated with blocking buffer (1x PBS containing 1% BSA, 5% Goat serum and 0.3% Triton X-100) for 30 min at room temperature. Then, the model or sections were incubated with primary antibodies diluted with blocking buffer overnight at 4°C. the model or sections were washed three times with PBS and incubated with the secondary antibodies conjugated with Alexa Fluor 488 or 568 (Thermo Fisher Scientific, 1:1000), and then incubated with Hoechst 33342 (Sigma-Aldrich). Following antibodies were used: anti-beta III Tubulin (Tuj1, Biolegend, 1:1000, 801202), anti-FOXG1 (Abcam, 1:1000, ab18259), anti-Tau-1 (Millipore, 1:1000, MAB3420), anti-Synapsin I (Millipore, 1:1000, AB1543), anti-MAP2 (Sigma-Aldrich, 1:1000, M4403), and anti-cleaved caspase 3 (Cell Signaling Technology, 1:500, 9664).

The bright field and fluorescent images were acquired with an inverted microscope (Olympus IX73) equipped with a CMOS camera (Zyla 4.2, Andor, or SR130M, Wraymer) or an automated inverted microscope (BZ-X800, Keyence).

Axon dispersion index was calculated as following. First, a rectangular region of interest was selected on a bright field image at the connection area between a chamber and a channel. Next, we run "Find edges" command on ImageJ to highlight axons. Then we generated an intensity distribution profile by "Plot profile" command. To remove background, mean value was subtracted

throughout the intensity profile, and negative values were replaced with zero. Lastly, we calculated variance of the profile and used the value as an index for dispersion of axons.

Electron microscopy

For surface structure analyses with scanning electron microscopy (SEM), the tissue was fixed with 1% glutaraldehyde in 0.1 M phosphate buffer (pH 7.4), and dehydrated in a graded series of ethanol. After sputter deposition of Pt with JFC-1600 (JEOL), surface images of the tissue were acquired with a scanning electron microscope JCM-6000Plus (JEOL).

For cross-section analyses with TEM, the tissue was fixed with 2.5% glutaraldehyde in 0.1 M phosphate buffer (pH 7.4) and post-fixed with 1% osmium tetroxide in 0.1 M phosphate buffer (pH 7.4) for 2 hours before dehydration. After embedded in epoxy resin, polymerized for 72 hours at 60°C, ultra-thin sections were prepared at 70 nm thickness with ultramicrotome (Leica UC7). Sections were stained with uranyl acetate and lead citrate for 10 minutes and examined with JEM-1400 Plus (JEOL). Detailed procedure for the TEM analysis was described previously (Shibata et al., 2015).

Calcium imaging

Calcium indicator dye Fluo-4 AM (CS22, Dojindo) was used as directed by the manufacturer. After extracted from a culture device, the tissue was incubated in loading buffer as recommended by the manufacturer for 30 min. After a wash with PBS, we transferred the tissue into BrainPhys medium (Stem Cell Technologies) supplemented with N2 and B27 supplements (ThermoFisher Scientific). A spheroid on one side within a tissue was located between two tungsten probe needles (SW6-1, Omniphysics Inc) positioned with micromanipulators (U-31CF, Narishige), and we examined alteration of fluorescent intensity triggered by electrical stimulations with an inverted microscope (IX73, Olympus) equipped with a CMOS camera (Zyla 4.2, Andor). Ten cycles of a positive square pulse for 2 ms, a negative square pulse for 2 ms, and a break for 2 ms at 6 – 8 V were applied with a stimulus generator (STG-4002, Multichannel systems) between a ground probe needle and the other probe needle. The experiments were performed at room temperature.

Electroporation of tissue

Neural spheroids cultured for 20 – 25 days were subjected to electroporation to visualize neuronal morphologies, especially extension of axons. For labeling with GFP, we electroporated spheroids using tweezer-type electrodes with platinum pads of a diameter of 5 mm (CUY650-P5, Nepa Gene). The electrodes were kept at distance of 2 mm, and the gap was filled with 30μL of DNA solution (total 1μg/μl consisting of 0.2 μg/μl pCAG-GFP (Matsuda and Cepko, 2007) and 0.8 μg/μl pBluescript/U6 plasmid (Gaudilliere et al., 2002)) in OPTIMEM (ThermoFisher Scientific) together with a spheroid. Three square pulses of electricity of 40V for 50 ms were applied to the

spheroid with an electroporator (NEPA21, Nepa Gene). After the electroporation, the spheroid was transferred back to the original medium supplemented with 40μM FUDR. After 24 hours, the spheroid was transferred to a microdevice with fresh media without FUDR. For knockdown of L1CAM, DNA solution including L1CAM RNAi construct (total 1μg/μl consisting of 0.2 μg/μl pCAG-GFP, 0.4 μg/μl L1CAM RNAi plasmid and 0.4 μg/μl pBluescript/U6 plasmid) or scrambled RNAi construct (total 1μg/μl consisting of 0.2 μg/μl pCAG-GFP, 0.4 μg/μl scrambled RNAi plasmid (de la Torre-Ubieta et al., 2010) and 0.4 μg/μl pBluescript/U6 plasmid) were used. The L1CAM RNAi plasmid was generated by cloning GCTGCTTTGCCAGCAATAAGAcaagttaacGCTTATTGCTGGCAAAGCAGCcttttg and aattcaaaaagGACATTGAATTTGAGGACAAGGAAAgttaacttgCTTCCTTGTCCTCAAATTCAATGTC into pBluescript/U6 as described (Gaudilliere et al., 2002).

Reference

de la Torre-Ubieta, L., Gaudillière, B., Yang, Y., Ikeuchi, Y., Yamada, T., DiBacco, S., Stegmüller, J., Schüller, U., Salih, D.A., Rowitch, D.*, et al.* (2010). A FOXO-Pak1 transcriptional pathway controls neuronal polarity. Genes Dev *24*, 799-813.

Gaudilliere, B., Shi, Y., and Bonni, A. (2002). RNA interference reveals a requirement for myocyte enhancer factor 2A in activity-dependent neuronal survival. J Biol Chem *277*, 46442-46446.

Lancaster, M.A., Renner, M., Martin, C.A., Wenzel, D., Bicknell, L.S., Hurles, M.E., Homfray, T., Penninger, J.M., Jackson, A.P., and Knoblich, J.A. (2013). Cerebral organoids model human brain development and microcephaly. Nature *501*, 373-379.

Matsuda, T., and Cepko, C.L. (2007). Controlled expression of transgenes introduced by in vivo electroporation. Proc Natl Acad Sci U S A *104*, 1027-1032.

Okita, K., Matsumura, Y., Sato, Y., Okada, A., Morizane, A., Okamoto, S., Hong, H., Nakagawa, M., Tanabe, K., Tezuka, K.*, et al.* (2011). A more efficient method to generate integration-free human iPS cells. Nat Methods *8*, 409-412.

Shibata, S., Murota, Y., Nishimoto, Y., Yoshimura, M., Nagai, T., Okano, H., and Siomi, M.C. (2015). Immuno-Electron Microscopy and Electron Microscopic In Situ Hybridization for Visualizing piRNA Biogenesis Bodies in Drosophila Ovaries. Methods Mol Biol *1328*, 163-178.